2021 IEEE International Conference on Systems, Man, and Cybernetics (SMC)
17-20 October, 2021. Melbourne, Australia

2021 IEEE International Conference on Systems, Man, and Cybernetics (SMC) | 978-1-6654-4207-7/21/$31.00 ©2021 IEEE | DOI: 10.1109/SMC52423.2021.9659101

Low-frequency Forced Oscillation Source Location for Bulk Power Systems: A Deep Learning Approach

Soumyabrata Talukder, Shaopeng Liu, Honggang Wang, and Gang Zheng

***Abstract*— Locating the source of low-frequency forced oscillation is an important aspect of bulk power system operation, and it facilitates operator's intervention to the faulty component and timely implementation of mitigation measures. In this paper, a novel deep learning-based forced oscillation source locator is proposed to infer the oscillation-source using data from phasor measurement units (PMU). The locator is trained offline using the spectral information extracted from the sliding-window time-series data from simulated PMU measurements over a range of randomly chosen oscillatory events. The effectiveness of the proposed method has been validated on the Western Electricity Coordinating Council (WECC) 179-bus test system, comparing with an existing energy-based method. Noise-robustness of the method has also been evaluated.**

***Index Terms*—Forced oscillation source, spectral data analysis, phasor measurement unit, deep learning.**

I. Introduction

Low-frequency forced oscillation (LFO) is a phenomenon in bulk power system, caused by the action of "exogeneous" low-frequency periodic disturbance. Such periodic disturbance typically intrudes into the system either from the generation end or from any of the connected loads. The enhanced real-time power system observability owing to the wide deployment of phasor measurement units (PMU), has unveiled the ubiquitous presence of LFO events across different power systems. Besides having detrimental effect on the life of the electro-mechanical components connected to the system, such LFO may even precipitate instability if the oscillation frequency is close to that of one of the system's natural modes, resulting in resonance [1]. As a mitigation measure, disconnecting the oscillation-source from the system has been accepted to be more effective in practice [2]. Hence, the problem of low-frequency forced oscillation source location (LFOSL) finds paramount importance in the practical bulk power system operation and has gained wide attention.

S. Talukder is with the Department of Electrical Engineering, Iowa State University, Ames, IA 50010 USA. This research was conducted during his internship at GE Research, NY USA (e-mail: talukder@iastate.edu).

S. Liu (corresponding author, ph: 518-387-4682; fax: 518-387-6845; email: sliu@ge.com) and H. Wang (e-mail: honggang.wang@ge.com) are with GE Research, Niskayuna, NY 12309 USA.

G. Zheng is with GE Digital, Vancouver, BC V7X1J1 Canada (e-mail: gang.zheng@ge.com).

The problem of LFOSL has been studied over many decades in the past [3]. Chen *et al*. [4] established the consistency between energy dissipation and generator damping torque, and the oscillation source is identified to be the component that contributes to non-dissipating energy flow, where the latter is estimated using PMU data. This method is restrictive in applications mainly due to its assumption of lossless network and *a priori* knowledge of the equilibrium. Maslennikov *et al*. in their dissipative energy flow (DEF) method [2] suggested certain approximations and enhancements on Chen's approach, making it more amenable for practical applications. The DEF method is reported to be deployed in the ISO New England system [5]. Feng *et al*. [6] built on the energy-based concept and introduced a two-step method to pinpoint the oscillatory source at the controller level in a generation plant.

In addition to the energy-based methods, there are a few other methods based on the data mining (DM) approach. OBrien *et al*. [7] introduced pattern mining and maximal variance ratio for LFOSL using supervisory control and data acquisition (SCADA) measurements. Meng *at al*. [8] employed k-nearest neighbors (KNN) for real-time LFOSL using PMU data at the generating plants, where data simulated from the power system model is used for offline learning of a *Mahalanobis* matrix. Chevalier *et al*. [9] introduced a *Bayesian* framework to infer LFO source by numerically estimating the optimal *a posteriori* from real-time PMU measurements in two stages, given an uncertain simplified *prior* model. Huang *et al*. [10] proposed a robust principal-component-analysis formulation of the LFOSL problem with the assumption that the matrix formed by the measurements at buses can be decomposed into a low-rank matrix and a sparse residue. Other than the energy-based and DM-based methods, Zhou *et al*. [11] proposed an LFO source tracer using the relative magnitude and phase of the transfer functions (between bus voltage angles of the pairs of buses) at the oscillation frequency by assuming the availability of the classical model parameters and the independence of responses due to each machine.

The power systems community is yet to converge on any of the proposed LFOSL methods, due to their restrictive assumptions, occasional inaccuracies, and/or implementational difficulties. In this paper, a deep learning-based alternate approach is proposed to locate the LFO source in real-time using frequency-domain data extracted from PMU measurements. The proposed deep-neural-network (DNN) is featured by a *convolutional LSTM* layer [12], where

the input is a temporal sequence of spectral snapshots (both magnitude and phase responses) computed by preprocessing the fixed-length sliding windows extracted from time-series PMU measurements including bus frequency, active and reactive power injections. The proposed approach is found to be more accurate than the energy-based method [4] on a simulated dataset generated using the WECC 179-bus test system. Moreover, it also shows robustness to measurement noise typically observed in PMU data.

The rest of the paper is organized as follows. Section II presents the proposed DNN-based framework and the frequency domain feature engineering. Section III discusses the experimental results on the WECC 179-bus test system and the comparison with an existing energy-based method. Section IV concludes the paper.

II. DNN-BASED LFOSL FRAMEWORK

The low-frequency forced oscillations (LFO) occur in bulk power system due to exogenous periodic disturbances that typically intrude into the system either from the generation end (e.g., through the mechanical input power or the signal received from the automatic voltage regulator) or from any of the connected loads due to the presence of cyclicity. Based on the amplitude of the LFO response typically observed in practice, both industry and academia assent to study such events by small-signal analysis, i.e., the system is linearized around the operating equilibrium to analyze its response to the low-frequency periodic disturbances. Although it is tempting to assume that such response should exhibit higher oscillation amplitude at and near the source-bus, the assumption is not valid if the frequency of oscillation is close to the frequency of any of the distant local, interarea modes of the linearized system causing resonance. In such case, the oscillation can be prevalent at a distant non-source bus corresponding to the local mode (respectively, a group of buses dominantly participating in the concerned interarea mode), making the LFOSL problem difficult. An excellent analytical treatment to the aforesaid possibilities is available in [10].

A. Overview of the Proposed Framework

The proposed DNN-based LFOSL framework is schematically shown in Fig. 1, which comprises of an "offline training" and a "real-time inference" phase. The "offline training" phase includes data collection, training of the proposed DNN, model selection through cross-validation and model evaluation on test dataset. The dataset can compose of field measurements of real LFO cases of a system, or simulated instances in absence of field measurements, or a combination of both. In the latter case, the user needs to provide the generator and line parameters of the system and an approximate nominal operating point. The proposed framework does not rely on strong modeling assumptions, and the exact load and generation schedule are not required. A time-domain simulation routine (TDS) is used to simulate multiple LFO cases, each with the system operating point and parameters perturbed randomly around the nominal condition, and with the oscillation source chosen randomly. The frequency-domain information extracted from the data together with the "one-hot-encoded" labels of LFO sources

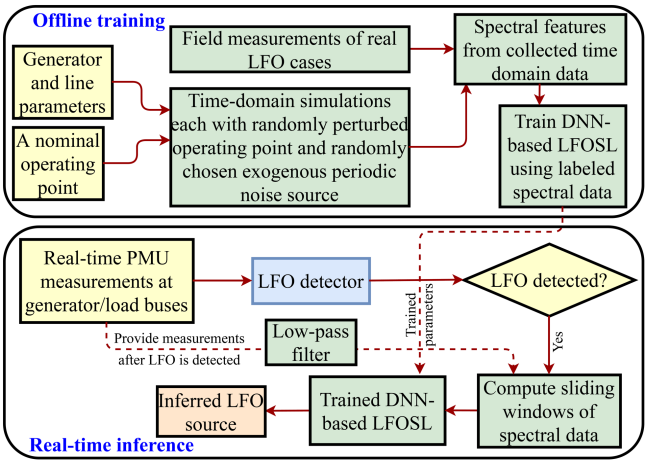

Fig. 1. Overall DNN-based LFOSL framework

are used to train, cross-validate and evaluate/test the DNN-based LFOSL. After it achieves the desired level of accuracy on the test data, the trained DNN-model is deployed to infer LFO source for the system based on real-time measurements.

In real-time inference phase, the trained and evaluated DNN-based LFOSL is used in tandem with an upstream LFO detector to infer LFO source from real-time measurements. The LFO detector is, however, beyond the scope of this paper, and one of the existing LFO detection techniques [13], [14] may be used for this purpose. Once the presence of LFO is detected, a sequence of fixed length sliding windows of measurements are extracted from the PMU samples. These are then denoised through a low-pass filter as the input to the a trained DNN to locate the LFO source.

B. Data Extraction and Spectral Feature Engineering

Let s_0 denote the discrete sample index corresponding to the detection instant of the upstream LFO detector. Assuming PMU measurements are available at every fixed time interval τ, the sequence of sample indices of the following N numbers of sliding L-samples long windows with fixed slide-hop length of h-samples is given by:

$$T_N := \{(s_0 + n.h) \oplus \{1,2,\dots,L\} \mid n \in \{0,\dots,N-1\}\} \quad (1)$$

where the operator $\oplus$ adds its left operand, a scalar, to each element of the right operand set. Here, the n^{th} element of the sequence T_N denotes the set of L sample indices corresponding to the n^{th} measurement window. Fig. 2.(a) schematically illustrates the extraction of N numbers of h-hop L-length sliding measurement windows from the PMU samples after an LFO detection, where the horizontal arrow denotes the progressing time axis, the vertical arrows denote the arriving PMU samples, and the n^{th} green box denotes the n^{th} measurement window.

Let there be M possible sources of LFO in the system, which may include the generators and the loads, and we use Q different measured quantities (e.g., frequency, power, etc.) at every possible source bus. Based on our experimental results, we suggest three measured quantities, namely, the frequency and the active and reactive power injections at the possible source buses to form the measurement set (i.e., $Q = 3$). The bus voltage magnitude is not recommended since an LFO

usually exhibits very low amplitude in voltage magnitude, and it may be difficult to reconstruct the LFO signal from noisy voltage measurements. The time-domain measurement set to be used as the raw input data is given by:

$$\mathcal{D}_{N,Q} \coloneqq \{D_{n,q} \in \mathbb{R}^{L\times M} \mid n \in \{0,\dots N-1\}, q \in \{1,\dots,Q\}\} \quad (2)$$

where the $(l,m)^{th}$ element of the matrix $D_{n,q}$ represents the measured value of the q^{th} quantity, measured at the l^{th} sample index of the n^{th} window, by the PMU placed at the m^{th} bus.

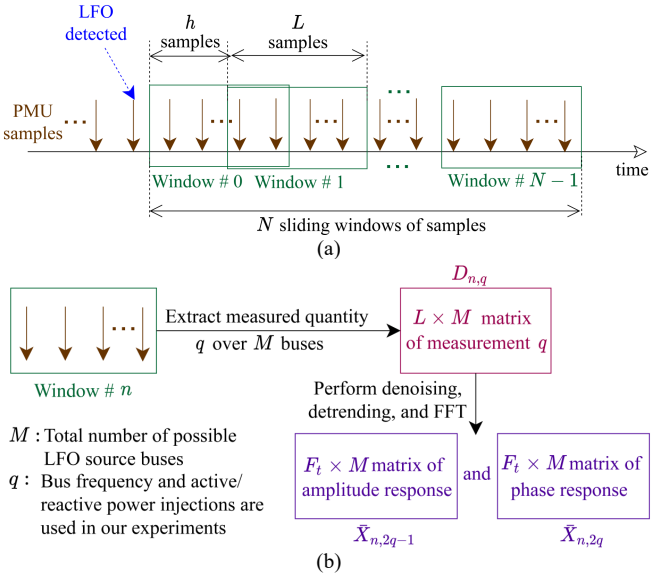

Fig. 2. Illustration of data extraction and preprocessing. (a) extraction of sliding windows from PMU data after detection of an LFO. (b) preprocessing steps performed on the measurements in the n^{th} window.

Any oscillatory response of a system is fundamentally characterized by a periodic signal of certain frequency, amplitude, and phase, or a superposition of multiple such signals. The spectral information extracted from an oscillatory time-series data contains these important attributes and hence, may be more causal compared to its raw time-domain form in data-driven identification of the LFO source. This motivates us to use the frequency-domain snapshots (comprising of both magnitude and phase responses) of the PMU measurements for DNN-based LFOSL. The LFOSL performance enhancement using frequency-domain input over its time-domain counterpart, has been substantiated through the experimental results presented in Section III.

Traditionally, fast Fourier transform algorithm (FFT) has been used to estimate the frequency response from finite samples of measurements of a signal. However, the key issue with FFT is the *leakage*, which is the error introduced if the value of $L.\tau$ is not an integer multiple of the actual time period of the underlying oscillation. Such error is unavoidable in FFT-based methods, where the oscillation frequency is not known a priori. Also, an oscillation in power system may comprise of multiple non-harmonic frequency components, in general, posing additional challenges. To minimize leakage, *Hanning* window [15] is applied by scaling the detrended L samples of a window by the corresponding Hanning coefficients. Moreover, the suggested sequence of N sliding windows (instead of only a single one) further makes the DNN-based LFOSL inference robust to the residual leakage that may still remain in the frequency response.

Fig. 2.(b) shows a schematic illustration of the spectral information extraction from the n^{th} measurement window. Each window contains Q different L-length time-series measurements over M possible LFO source buses. The subsequent preprocessing is performed individually on each measurement matrix $D_{n,q}$, i.e., the measurements of quantity q over M buses extracted from the window, for all $q \in \{1,\dots,Q\}$. For each bus, the frequency response of the measured quantity q is estimated by running FFT on the Hanning-scaled, denoised, and detrended version of the time-domain measurements. Only the right-sided frequency response is considered, generating magnitudes and phases over a range of $\lfloor L/2 \rfloor + 1$ discrete frequencies denoted by F. Since frequencies lower than $1/L.\tau$ Hz cannot be reliably estimated using the L-length window, the truncated frequency range $F_t \subset F$ that includes the frequencies equal or above $1/L.\tau$ Hz is used. By stacking the computed magnitude (respectively, phase) responses corresponding to the respective M buses as the columns, we form the matrix $\bar{X}_{n,2q-1}$ (respectively, $\bar{X}_{n,2q}$), which contains the spectral information pertaining to the q^{th} measured quantity over all possible LFO source buses, for the n^{th} window. Accordingly, the overall frequency domain data that we compute for a given LFO scenario, is compactly denoted by the following set:

$$\bar{\mathcal{X}}_{N,2Q} \coloneqq \{\bar{X}_{n,ch} \in \mathbb{R}^{F_t\times M} \mid n \in \{0,\dots N-1\}, ch \in \{1,\dots,2Q\}\} \quad (3)$$

where the subscript ch corresponds to the "input channel" of our DNN. A normalized version of $\bar{\mathcal{X}}_{N,2Q}$, denoted $X_{N,2Q}$, is used as the input to the DNN model, where $2Q$ is the total number of input channels each of dimension $F_t \times M$, and N is the length of the input sequence.

Fig. 3 provides a schematic summary of our data-preprocessing pipeline. The set $\mathcal{D}_{N,Q}$ contains $N.Q$ numbers of $L \times M$ matrices of time domain data, each of which (e.g., $D_{n,q}$) is transformed into a corresponding frequency domain pair (e.g., $\bar{X}_{n,2q-1}$, $\bar{X}_{n,2q}$) of dimension $F_t \times M$, forming the intermediate set $\bar{\mathcal{X}}_{N,2Q}$, which is finally normalized to $X_{N,2Q}$.

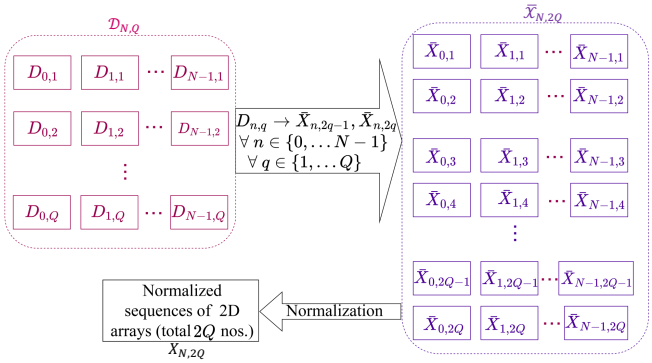

Fig. 3. Illustration of the formation a $2Q$ channeled sequential input for the convolution LSTM layer from the h-hop L-length N sliding windows of Q measurements, for a single LFO scenario.

It is practical to consider only a single source of LFO while generating each simulation-based LFO scenario, since the

coexistence of multiple simultaneous LFO sources is unlikely. The true LFO source for a given scenario is represented by an M-dimensional one-hot encoded vector y. The duple $\{X_{N,2Q}, y\}$ forms a single data instance for our DNN.

C. Proposed DNN Architecture for LFOSL

The spectral feature engineering introduced in the previous subsection enables usage of a *convolutional LSTM* [12], which is capable of spatiotemporally correlate the spectral features underlying the oscillatory measurements, facilitating an effective supervised learning to predict the LFO source. Our proposed DNN architecture is shown in Fig. 4.

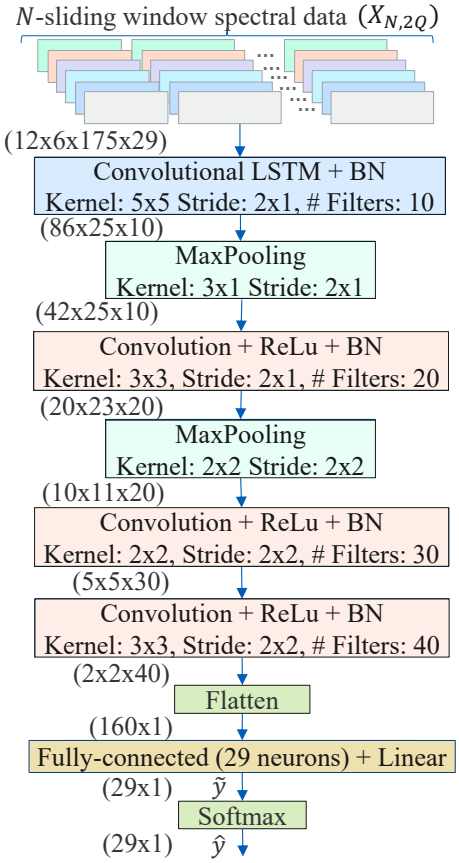

Fig. 4. Deep-neural-network architecture proposed for LFOSL

The first layer is a 2-D *convolutional LSTM* that takes the N-length sequence of $2Q$ channeled frequency domain snapshots of the system's response each of $F_t \times M$ dimension as its input, and outputs a non-sequential temporally (along n-axis), spectrally (along the axis of $f \in F_t$) as well as spatially (along m-axis) correlated summary. The next three 2-D *convolutional* layers extract features from this summary with *ReLu* activation functions. A *maxpooling* layer is added after each of the first two layers to make the learned features robust to local perturbations and to reduce the feature size for the deeper layers of the DNN enabling lower-level feature learning. The output layer is a *fully-connected* linear layer with the number of neurons identical to the possible number of LFO sources M, and receives 1-D data after appropriate reshaping (as shown in Fig. 4 by the *flatten* operation) of the previous layer's output. A *softmax* function is applied to the computed output $\tilde{y} \in \mathbb{R}^M$ to map the latter into a M dimensional probability vector $\hat{y}$. The index corresponding to the maximum valued element of $\hat{y}$ points to the LFO source as inferred by the DNN. The data dimensions at the output of the hidden layers, as mentioned within round brackets in Fig. 4, and the dimensions of the convolution kernels and strides, correspond to those used in the experimental results in Section IV. The Kullback-Leibler divergence (identical to the cross-entropy since y is one-hot encoded) of the estimated data distribution (e.g., $\hat{y}$ given $X_{N,2Q}$) to the true one (i.e., y given $X_{N,2Q}$) is minimized during the training of the DNN model, which for a batch-size of B is given by:

$$\mathcal{L} := \frac{1}{B}\sum_{b=1}^{B}\sum_{m=1}^{M} y_{b,m}\log\left(\frac{y_{b,m}}{\hat{y}_{b,m}}\right) \tag{4}$$

where the subscripts b and m denote the data instance number in a batch and the output index respectively. Since the DNN model is trained with back-propagation using the whole training data split into multiple batches, *batch-normalization* (BN) [16] is used after each of the first four layers, which helps to reduce the internal covariance shift during training.

III. Case Study on WECC 179-bus System

A. Data Simulation & Preprocessing

Although the IEEE Taskforce has made available several manually crafted LFO data instances simulated on WECC 179-bus test system [17], more data is needed to carry out an effective supervised learning training process. For automated data generation using the same WECC 179-bus model, the TDS-routine of the open-source tool PSAT [18] is extended for LFO simulations and coupled with a Siemens PTI PSS/E-format power system model data-parser, extending an interface available with MATPOWER [19].

A total of 4553 data instances were generated by repeatedly running the TDS routine. In each TDS case, the operating point was set by solving power-flow after perturbing the load by u%. The value u was randomly chosen independently for each connected load. The net change in the active power demand (if any) was assumed to be shared among all the generators according to their nominal proportion. The diverging power-flow cases or the ones having any unstable small-signal mode were discarded. The 29 generators in the system were considered to be the possible LFO sources, i.e., $M = 29$. During TDS, the exogenous disturbance was simulated by applying additive periodic noise of frequency fr and magnitude p% of that of the nominal signal (or a superposition of at most two such noises), either to the mechanical power input or to the q-axis internal voltage of one of the generators. The number of frequency components in the disturbance, their waveshape, and the quantities fr and p were randomly selected in each TDS case independently. Such disturbances were triggered at 10 seconds during the simulation and remained thereafter.

Although the availability of an upstream LFO detector is assumed, it is recognized that the detection latency of such a detector may vary from one LFO case to another and cannot

be ascertained a priori. Hence, the sample index s_0 corresponding to LFO detection was randomly chosen from the samples within the simulation interval of [20, 25] seconds for each TDS case. The specifics of the randomly chosen parameters are enumerated in Table I. It was noted that a few LFO led to short-term angle instability, which might occur if an LFO-caused resonance drifts the operating-point out of the stability region of the dynamic equilibrium. Such cases were discarded from the simulation dataset since the goal was to generate a dataset with cases exhibiting sustained LFO. In practical applications, the parameters of Table I needs to be set carefully so that the generated data represent real-life operating scenarios well enough, in order to achieve the desired generalization capability of the DNN model.

TABLE I
Randomly Selected Parameters in each TDS

Parameter Name	Range/set of Random Choices
Load perturbation (u)	[0, 20] % of nominal value
Source of LFO disturbance	Generator # {1, 2, …, 29}
Signal to add disturbance on	{Mechanical power input, q-axis internal voltage}
Disturbance frequency (fr)	[0.1, 1.5] Hz.
Disturbance magnitude (p)	[5, 10] % of nominal signal magnitude
No. of frequency components in a disturbance	{1, 2}
Disturbance waveshape	{square, sinusoidal}
LFO detection instant	[20, 25] sec.

The data preprocessing was performed using the Python package Numpy (version 1.18.5). To prepare the input data $X_{N,2Q}$, a window-length of $L = 350$ was chosen with sampling interval $\tau = 30$ msec., so that a frequency component of as low as 0.1 Hz could be estimated by FFT. The number of measured quantities $Q = 3$ comprised of bus frequency injected active and reactive powers. A slide-hop length $h = 50$ samples was chosen with the total slides of $N = 12$. Each preprocessed input $X_{N,2Q}$ to the DNN model has the dimension of $12 \times 175 \times 29 \times 6$.

B. DNN Model Training and Evaluation

The DNN construction and its training were implemented using the Python-package TensorFlow (version 2.3.1). The 10% of the 4553 preprocessed data instances were randomly selected and kept aside as test dataset to evaluate the generalization capability of the selected DNN models. The rest was randomly split for training and cross-validation in 8:2 proportion prior to each training trial. The loss computed on the cross-validation dataset was used to select the best model, searched by tuning the model hyper-parameters. Adam [20], the adaptive momentum-based stochastic gradient decent algorithm was used to minimize the loss function (4) by backpropagation. A dropout rate of 25% was used to avoid overfitting on the training data. The training was continued for 150 epochs with a batch-size of 200, while the batch-formation was performed randomly after each epoch of training.

C. Performance Comparison of DNN-based Methods

To compare the performance of the proposed Convolutional LSTM-based DNN architecture with frequency domain input, the alternative approaches include using time-domain PMU measurements as inputs and using a regular LSTM-based [21] classifier. Table II shows the accuracies of three different DNN-based models used for the performance comparison: Case I is the proposed Convolutional LSTM model (see Fig. 4 for the hyper-parameters of the selected best-performing model) with frequency-domain data as inputs, Case II uses time-domain data as the Convolutional LSTM model inputs, and Case III uses the time-domain data on a regular LSTM-based DNN model. The training/validation loss of Case I, Case II and Case III are presented in Fig. 5.

TABLE II
Comparison of Performance of Different DNNs

Cases	DNN Architecture	Input Type	Training Accuracy (%)	Validation Accuracy (%)	Test Accuracy (%)
Case I (proposed)	Convolutional LSTM	Frequency domain	99.93	98.71	98.59
Case II	Convolutional LSTM	Time Domain	86.61	72.77	72.82
Case III	Regular LSTM	Time Domain	96.97	87.65	88.34

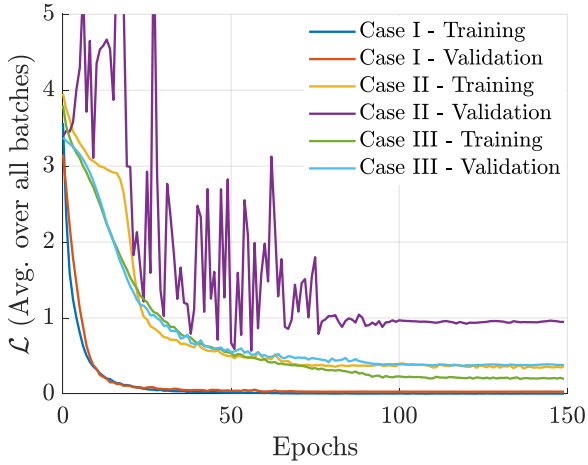

Fig. 5. Training and validation loss (averaged over the respective batches) over 150 training epochs for the three respective cases, accuracies of which are reported in Table II. Note that the validation losses are computed after completion of the respective training epochs.

Specifically, Case II uses a convolutional LSTM-based DNN with the stride on the convolutional LSTM increased to 4×1, which makes the output data dimensions of the hidden layers to remain the same to those of Case I. The input data is the normalized version of $D_{N,Q}$ of (2) as opposed to $X_{N,2Q}$ used for Case I. As seen in Table II and Fig. 5, Case II did not perform well compared to Case I model. Case III model employs a regular LSTM cell with output dimension 50 with 50% drop out, followed by a fully connected linear layer of 29 neurons with the softmax operator at the output. The measurements were first down-sampled to match 0.3 sec. sample interval, and then the sequence of 70 such samples (starting from s_0) of Q-dimensional normalized measurements were used as the input. It is found that increasing model parameters or reducing the drop-out percentage in the LSTM model would cause overfitting of the model at the early stage of training and worsen the final validation loss. In addition, the proposed convolutional LSTM architecture of Case I is

recommended over the regular LSTM due to the presence of multiple fully-connected layers embedded in a single LSTM cell, which increases its model-complexity (in terms of the number of parameters) as the power system under study becomes larger (due to increase in the input dimension). This may impose restrictions on the scalability of the regular LSTM-based model, whereas convolutional LSTM, with the convolution kernel size being invariant to the value of M (hence, invariant to the power system's size), does not face such scalability issue.

The noise robustness of the Case I DNN model has been evaluated after adding 45 dB white noise to the test dataset. Specifically, all Q measurement quantities at each sample instant were perturbed independently by 45 dB random noise, , which has been shown to be adequate to model noisy PMU measurements [22]. A stable digital Butterworth low-pass filter of order 6 with corner frequency of 1.5 Hz was applied on each time-domain window. An accuracy of 91.81% was achieved on the noise-corrupted test dataset, demonstrating the noise robustness of the proposed approach.

D. Comparison with Energy-based Method

The energy-based method in [4] has also been implemented to compare with the results from the proposed DNN approach. The energy-based method has shown an LFOSL accuracy of 96.4% on the simulated data. This further validates the effectiveness of the proposed DNN approach as the results in Case I have shown comparable and better performance.

It is noted that the energy-based method is restrictive in general, due to its assumption of lossless network, constant impedance load and a priori knowledge of the equilibrium, but it has the advantage of not requiring any knowledge of the system's dynamic model. In contrast, our proposed framework does not have any of the restrictions as posed by the energy-based method and does not require a dynamic model with accurate load and generator dispatch schedule for practical applications.

IV. Conclusion

A deep learning-based approach is presented for low-frequency forced oscillation source location (LFOSL) for bulk power systems. The proposed deep neural network (DNN) model takes a sequence of spectral snapshots (both magnitude and phase responses) extracted from the sliding-window time-series of PMU data as input. The proposed method was implemented on the WECC 179-bus test system, which was used to simulate various forced oscillations cases (a total of 4553 cases) for the purpose of supervised learning. The results showed that the proposed approach is more accurate in locating the source of oscillation than an existing energy-based method on the unseen dataset and is adequately noise robust with 91.81% LFOSL accuracy on data with white noise of 45 dB power level. Our results also demonstrated that the DNN trained using frequency domain data outperforms those trained using time domain data for the same objective. Our future work will focus on investigation of natural oscillation source location for bulk power systems using deep learning-based methods.

V. References

[1] S.A.N. Sarmadi, V. Venkatasubramanian and A. Salazar, 2016. Analysis of November 29, 2005 western American oscillation event. *IEEE Transactions on Power Systems*, 31(6), pp.5210-5211.

[2] S. Maslennikov, B. Wang and E. Litvinov, 2017. Dissipating energy flow method for locating the source of sustained oscillations. *International Journal of Electrical Power & Energy Systems*, 88, pp.55-62.

[3] M. Ghorbaniparvar, 2017. Survey on forced oscillations in power system. *Journal of Modern Power Systems and Clean Energy*, 5(5), pp.671-682.

[4] L. Chen, Y. Min and W. Hu, 2012. An energy-based method for location of power system oscillation source. *IEEE Transactions on Power Systems*, 28(2), pp.828-836.

[5] S. Maslennikov and E. Litvinov, 2020. ISO New England Experience in Locating the Source of Oscillations Online. *IEEE Transactions on Power Systems*.

[6] S. Feng, B. Zheng, P. Jiang and J. Lei, 2018. A two-level forced oscillations source location method based on phasor and energy analysis. *IEEE Access*, 6, pp.44318-44327.

[7] J. OBrien, T. Wu, V. Venkatasubramanian and H. Zhang, 2017, January. Source location of forced oscillations using synchrophasor and scada data. In *Proceedings of the 50th Hawaii International Conference on System Sciences*.

[8] Y. Meng, Z. Yu, D. Shi, D. Bian and Z. Wang, 2018, April. Forced oscillation source location via multivariate time series classification. In 2018 *IEEE/PES Transmission and Distribution Conference and Exposition (T&D)* (pp. 1-5).

[9] S. Chevalier, P. Vorobev and K. Turitsyn, 2018. A bayesian approach to forced oscillation source location given uncertain generator parameters. *IEEE Transactions on Power Systems*, 34(2), pp.1641-1649.

[10] T. Huang, N. M. Freris, P. R. Kumar and L. Xie, 2020. A Synchrophasor Data-Driven Method for Forced Oscillation Localization Under Resonance Conditions, *IEEE Transactions on Power Systems*, 35(5), pp. 3927-3939.

[11] N. Zhou, M. Ghorbaniparvar and S. Akhlaghi, 2017, February. Locating sources of forced oscillations using transfer functions. In 2017 *IEEE Power and Energy Conference at Illinois,* pp. 1-8.

[12] X. Shi, Z. Chen, H. Wang, D.Y. Yeung, W.K. Wong and W.C. Woo, 2015. Convolutional LSTM network: A machine learning approach for precipitation nowcasting. *Advances in neural information processing systems*, 28, pp.802-810.

[13] X. Wang and K. Turitsyn, 2015. Data-driven diagnostics of mechanism and source of sustained oscillations. *IEEE Transactions on Power Systems*, 31(5), pp.4036-4046.

[14] R. Xie and D. Trudnowski, 2015, July. Distinguishing features of natural and forced oscillations. In 2015 *IEEE Power & Energy Society General Meeting* (pp. 1-5).

[15] J.F. Hauer and F. Vakili, 1990. An oscillation detector used in the BPA power system disturbance monitor. *IEEE Transactions on Power Systems*, 5(1), pp.74-79.

[16] S. Ioffe and C. Szegedy, 2015. Batch normalization: Accelerating deep network training by reducing internal covariate shift. arXiv preprint arXiv:1502.03167.

[17] S. Maslennikov, B. Wang, Q. Zhang and E. Litvinov, 2016, July. A test cases library for methods locating the sources of sustained oscillations. In 2016 *IEEE Power and Energy Society General Meeting (PESGM)* (pp. 1-5).

[18] F. Milano, 2005. An open source power system analysis toolbox. *IEEE Transactions on Power systems*, 20(3), pp.1199-1206.

[19] R.D. Zimmerman, C.E. Murillo-Sánchez and D. Gan, 1997. MATPOWER: A MATLAB power system simulation package. Manual, Power Systems Engineering Research Center, Ithaca NY, 1.

[20] D.P. Kingma and J. Ba, 2014. Adam: A method for stochastic optimization. arXiv preprint arXiv:1412.6980.

[21] S. Hochreiter and J. Schmidhuber, 1997. Long short-term memory. *Neural computation*, 9(8), pp.1735-1780.

[22] M. Brown, M. Biswal, S. Brahma, S.J. Ranade and H. Cao 2016, July. Characterizing and quantifying noise in PMU data. In 2016 *IEEE Power and Energy Society General Meeting (PESGM)* (pp. 1-5).